A Planar Shaped-Beam Antenna for Indoor Wireless LAN Access Points

Ruey Bing Hwang, *Senior Member, IEEE*, and Ta Chun Pu

***Abstract*—A planar antenna is described that is made up of a line source embedded in a structure containing a metal reflector and a dielectric layer coated with metal strips. We have fabricated and measured the radiation characteristics, including the return loss and radiation pattern. In addition to the experimental studies, the rigorous mode-matching method incorporating the equivalent principle was employed to calculate the electromagnetic fields in the structure and the far-field radiation pattern, as well. Besides, the sensitivity analyses for the radiation pattern against the variations on the structure parameters and relative dielectric constant were carefully carried out. The good agreement between the measured and calculated results was found. Combining the leak-waves and space-wave radiating from this structure, such a linearly polarized antenna can radiate a rectangular footprint of uniform electric-field strength, with 9% bandwidth around 11.4 GHz.**

***Index Terms*—Metal strips array, planar radome, shaped-beam antenna, uniform coverage.**

I. Introduction

THE highly shaped-beam antenna was first developed to give approximately uniform coverage of the earth from satellite antenna [1]–[3]. Recently, the similar requirement but different application; that is, the indoor high speed data transmission: wireless local area networks operating in the millimeter wave, again attracts considerable attentions [4]–[7]. Due to the critical specification in link budget, the transmitted power has to be efficiently distributed over the coverage; the spatial fluctuation of the field strength has to be as small as possible (within 6 dB) within the defined coverage area, whereas outside the coverage the field strength has to fall off rapidly. A shaped reflector antenna for 60-GHz wireless LAN access point was developed [5], [6]. A circular footprint having the deviation from the average field strength less than 2.5 dB in the far field was reported [5]. They comment that the practical imperfections such as axial and lateral feed displacement and mispointing of the feed on top of effects due to blockage by the feed-horn may contribute to spatial field variations [5]. The prototype Plexiglas dielectric lens shaped antenna was developed in indoor wireless LAN application [7].

In this research, the structure under consideration is a line (current) source sandwiched between a metal reflector and dielectric slab (planar radome) coated with metal-strip array. The electromagnetic field excited by the line source is shaped after transmitting through the planar radome. In fact, such a class of structures is very similar to a grating antenna; the line source used here attempts to excite the guided waves in the structure. In view of the presence of metal grating (hereafter, the metal grating refers to metal strips array), the guided wave becomes leaky wave radiating into free space. Since the line source is placed in the center of the structure, it excites the waveguide modes propagating along the $\pm x$ direction, resulting in the occurrence of two leaky waves. Combining the two leaky wave peaks and the radiation directly from the line source (space wave), a desired illumination pattern was synthesized.

Notably, the present antenna can not have the radiation characteristics (circular footprint and circular polarization) reported in the literature; however, the contribution of this research is to verify the design of highly shaped-beam antenna using the properties of leaky-wave and space-wave radiating from the structure under consideration. Such a type of leaky-wave structures has been studied intensively for their radiation characteristics by many researchers, and their applications mostly focused on the directional antenna design. To mention a few, the full-wave analysis for the one- or two-dimensional (1-, 2-D) metallic periodic structures excited by a line source was carried out [9], [10]. The mode excitation from sources in 2-D electromagnetic bandgap waveguide using the array scanning method was studied [11]. The directive radiation from the structure with a line source in a meta-material slab made from the conducting cylinders array was analyzed using both the full-wave method and the homogeneous slab model [12]. The radiation characteristics of a leaky-wave antenna constructed by a periodic array of metal patches on a grounded dielectric substrate were investigated [13]. Moreover, radiation at broadside for the similar structure in [13] was studied based on a simple transverse equivalent network model of the structure [14]. In addition to the metallic periodic structures used in the leaky-wave antenna design, the dielectric periodic structures taken as the antenna superstrate also were widely employed; for example, a parallel plate photonic bandgap and periodic medium waveguides was investigated [15]; a planar electromagnetic bandgap antenna design with periodical dielectric layers above a ground plane and excited by a printed patch antenna was verified to be able to enhance the gain and radiation bandwidth [16], [17]. A new resonator antenna consisting of a woodpile electromagnetic bandgap material and a metallic ground plane was developed to have highly directive radiation pattern [18].

In addition to the fabrication and measurement of the shaped-beam antenna, we have carried out the theoretical studies for investigating its radiation characteristics. The purpose is to lay a rigorous mathematical foundation for the

Manuscript received June 6, 2006; revised March 2, 2007. This work was supported in part by the Ministry of Education under Contract MOE ATU Program and by the National Science Council under Contract NSC 95-2221-E-009-045-MY3.

The authors are with the Department of Communication Engineering, National Chiao Tung University, Hsinchu, Taiwan, Republic of China (e-mail: raybeam@mail.nctu.edu.tw).

Digital Object Identifier 10.1109/TAP.2007.898591

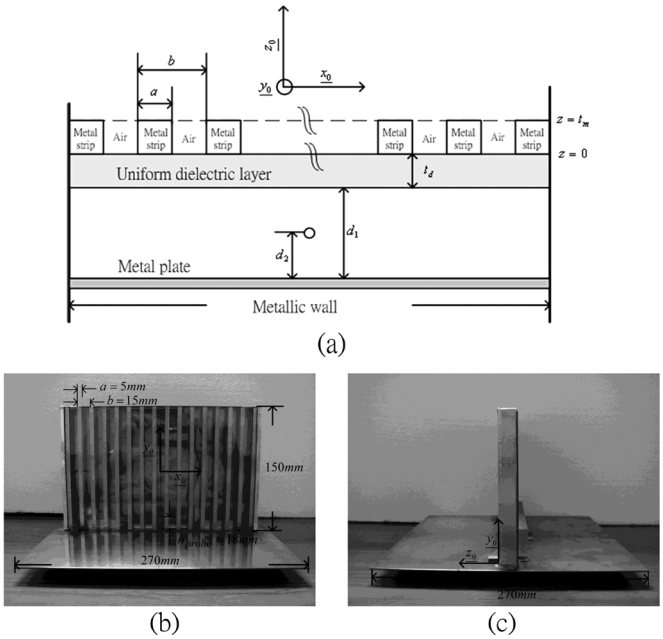

Fig. 1. The planar shaped-beam antenna: (a) structure configuration and parameters assignment, (b) front view, and (c) side view.

analysis of this class of shaped-beam antennas. Stress is placed on network representations to establish physical pictures of the wave processes and yield insight; besides, a systematic microwave network approach is employed. This building-block approach first breaks the cross-sectional geometry into constituent parts, analyzes each part rigorously, and then combines them into an input-output relation through the continuous of tangential electric- and magnetic- fields at the junction discontinuities. As shown in Fig. 1, the configuration of the antenna contains an oversized metallic waveguide filled with a dielectric layer coated with metal grating, a metal reflector, and a line source acting as excitation. To treat each of junction discontinuities between an oversized waveguide and sub-waveguides, the method of mode matching is employed. Thus, the structure is analyzed as a rigorous boundary value problem, so that the field distributions on the outmost surface can be determined accurately. Then, far-field radiation patterns from the outmost surface are obtained by calculating the Kirchhoff-Hygens radiation integrals for each individual modes and summing their contributions [8].

The organization of this paper is described as follows. In the next section, we will introduce the structure configuration and parameters of the planar shaped-beam antenna. The mathematical formulations, including the mode-matching method and equivalent principle, used for obtaining the far-field radiation pattern will be highlighted in the third section. The measured and numerical results obtained from our codes will be demonstrated in the fourth section. Finally, in the fifth section, some remarks will be given to conclude this paper.

II. Structure Configuration

As shown in Fig. 1(a), the antenna under consideration contains an air separator with thickness denoted as d_1, sandwiched between a metal plate and metal strips array (metal grating) coated on a dielectric substrate. The width, length and thickness of each metal strip are a, l and t_m, respectively. The period of the metal strip array is b. The dielectric layer has the thickness t_d and relative dielectric constant ε_r. The structure is excited by a line source made up of a coaxial probe. The distance from the line source to the metal plate is d_2. The width of the antenna is $(N-1)b+a$, where N is the number of periods along the x direction. To have a symmetric radiation pattern in the forward direction, the line source is placed at the center along the x direction.

III. Method of Analysis

For the theoretical formulation, since the length of the structure along the y-direction is greater than five times of the operation wavelength, the structure is assumed to have no electromagnetic fields variation along the y the direction. Accordingly, the electromagnetic field problem could be regarded as a two-dimensionally boundary-value problem. The individual polarization (E_y mode) is considered only, without dealing with the cross-polarization problem. Returning to Fig. 1(a), since the structure has only one open end along the $+z$ direction, the radiation far-field can be approximately calculated by the equivalent sources, including the electric- and magnetic- source, induced on the outmost surface of the metal grating. To resolve the electromagnetic fields on the outer surface of metal grating, we have to solve the electromagnetic fields in the parallel-plate waveguide (PPWG) consisting of multiple junction discontinuities. Because that the structure consists of many typical PPWGs whose mode functions are well known (the unknown to be determined are the modal amplitudes), the mode-matching method was employed to formulate the electromagnetic boundary-value problem. The electric field is assumed to be vanished in the metal strip (perfect electric conductor), thus, the region between two adjacent metal strips can be regarded as a sub-PPWG. Consequently, the electromagnetic fields are expressed in term of the summation of PPWG modes. By matching the tangential electric and magnetic fields across the discontinuities between the sub-PPWGs and the oversized PPWG, the original electromagnetic fields problem can be converted into the cascades of transmission line networks including an excitation current source. Therefore, the modal voltage and current everywhere are determined by solving the transmission-line network.

The representation of the electric and magnetic fields within a uniform waveguide can be reformulated into an engineering description in terms of an infinite number of modal voltages and currents. The variation of each modal voltage and current along the guide axis is described in terms of the corresponding variation of voltage and current along an appropriate transmission line. The description of the entire field within the guide is thereby reduced to the description of the electrical behavior on an infinite set of transmission lines.

Since the mathematical procedure of mode-matching method was well known in microwave engineering, we listed some important equations while the detail mathematical procedures can be found in the Appendix.

As aforementioned, the metal strip is assumed to have infinite conductivity; thus, the electric fields exist in the sub- and oversized-PPWG region. The electric and magnetic fields in the

oversized-PPWG or sub-PPWGs can be expressed in terms of the superposition of PPWG modes, which are given here

$$E_y(x,z) = -\sum_{n=1}^{\infty} \overline{V}_n^{(i)}(z)\overline{\phi}_n^{(i)}(x) \quad x \in i\text{th aperture} \tag{1}$$

$$H_x(x,z) = \sum_{n=1}^{\infty} \overline{I}_n^{(i)}(z)\overline{\phi}_n^{(i)}(x) \quad x \in i\text{th aperture} \tag{2}$$

$$\text{with } \overline{\phi}_n^{(i)}(x) = \sqrt{\frac{2}{w_i}} \sin\frac{n\pi(x-x_i)}{w_i} \quad x \in [x_i, x_i + w_i] \tag{3}$$

where x_i and w_i are the start position and width of the ith aperture, where the Vs and Is denote the voltage and current waves in each parallel-plate waveguide, which satisfy the transmission line equations along the z direction given as follows:

$$\frac{dV_n(z)}{dz} = -jk_{zn}Z_nI_n(z) \tag{4}$$

$$\frac{dI_n(z)}{dz} = -jk_{zn}Y_nV_n(z) \tag{5}$$

where the k_{zn} and Z_n (Y_n) are the propagation constant and impedance (admittance) along the z-direction, which are written as

$$k_{zn} = \sqrt{k_o^2\varepsilon_r - (n\pi/s)^2} \tag{6}$$

$$Z_n = \omega\mu_o/k_{zn}. \tag{7}$$

After matching the tangential electric and magnetic fields at the discontinuity $(z = t_m)$ across the uniform layer and metal grating, the voltage and current waves in respective regions are related by the following:

$$V_m\left(t_m^+\right) = \sum_{i=1}^{N}\sum_{n=1}^{\infty} \left\langle \phi_m(x) \middle| \overline{\phi}_n^{(i)}(x) \right\rangle \overline{V}_n^{(i)}\left(t_m^-\right) \tag{8}$$

$$\overline{I}_m^{(i)}\left(t_m^-\right) = \sum_{n=1}^{\infty} \left\langle \phi_n(x) \middle| \overline{\phi}_m^{(i)}(x) \right\rangle I_n\left(t_m^+\right) \tag{9}$$

$$\overline{V}_m^{(i)}\left(t_m^-\right) = \sum_{n=1}^{\infty} \left\langle \phi_n(x) \middle| \overline{\phi}_m^{(i)}(x) \right\rangle V_n\left(t_m^+\right) \tag{10}$$

with the notation

$$\left\langle \phi_m(x) \middle| \overline{\phi}_n^{(i)}(x) \right\rangle = \int_{x_i}^{x_i+w_i} \phi_m(x)\overline{\phi}_n^{(i)}(x)dx \tag{11}$$

where the parameter i denotes the index number of the ith aperture in the metal grating and the parameter N is the number of apertures. The parameters Vs and Is are the modal-voltage and current amplitudes in the oversized waveguide, and ϕ(x) is the modal function along the x direction. Equations (8)–(10) define the relations of the modal-voltage and current between the oversized- and sub-PPWGs. By applying the same procedure at the interface $z = 0$, we could obtain the similar input-output relation for the modal-voltage and current.

The next step to be dealt with is the excitation problem. The line source embedded in the air separating layer can also be expressed in terms of the superposition of PPWG modes, each of which is viewed as the incident mode for the scattering analysis. The modal voltage waves at the position of line source relate to the excitation current amplitude and the input impedance of each PPWG mode looking upward and downward from the position of excitation [see (A17)]. Furthermore, the transmitted voltage (and current) waves of each waveguide mode from the position of excitation source to the outmost surface of the metal grating is determined by cascading the input-output relation derived previously. After taking the superposition for these transmitted voltage and current waves contributed by respective incident waveguide mode, the overall electric and magnetic fields distribution on the outmost surface of the antenna are obtained. Since this structure has only one open end, the backward and sideward radiations shall be negligible. The radiation far field in the forward direction is determined using the 2-D Fourier transform of the aperture field on the outer surface of the metal grating. The equivalent- electric and magnetic currents on the outer surface are given as follows:

$$M_x(x) = -\sum_{n=1}^{\infty} V_n^{(s)}\left(t_m^+\right)\phi_n(x) \tag{12}$$

$$J_y(x) = \sum_{n=1}^{\infty} I_n^{(s)}\left(t_m^+\right)\phi_n(x) \tag{13}$$

where V's and I's in (12) and (13) represent the voltage and current waves of each PPWG mode of the oversized PPWG on the outmost surface. Notice that, in this research, we assumed that the electromagnetic fields have no variation along the y direction. Therefore, in the far-field radiation calculation, the equivalent sources were supposed to be uniform along the length of the radiating aperture, while the electric and magnetic fields are assumed to be vanished outside the radiation aperture.

IV. Numerical and Experimental Results

Fig. 2 depicts the radiation pattern of the shaped-beam antenna developed in this paper. This planar antenna was fabricated by printing the copper foil, with thickness 0.05 mm, on a dielectric substrate (acrylic) with thickness 1.86 mm and relative dielectric constant $\varepsilon_r = 2.59$. The excitation probe was placed between the metal grating and the metal plate, where the distance to the metal plate is 3 mm. The width, length and period of the metal strip are 5, 150, and 15 mm, respectively. The number of metal strips is 16. The radiation pattern was measured in an anechoic chamber using vector network analyzer HP 8722D and broadband standard-gain horn antenna.

As we have known, the translation of power illumination pattern function with smooth transition ([5, Eq. (9)]) to the far field in polar coordinates yields the $\sec^2$ pattern. From Fig. 2(a)–(c),

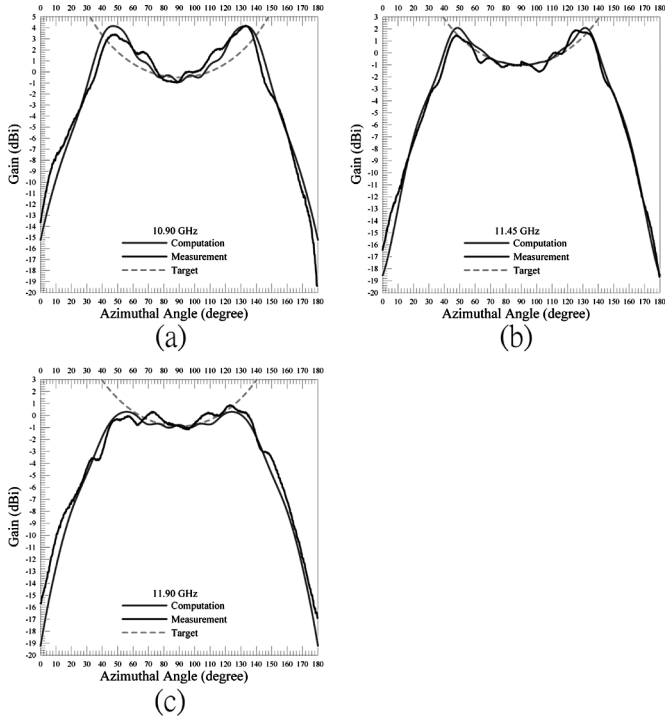

Fig. 2. Measured, computed and target patterns of the shaped-beam antenna ($\varepsilon_r = 2.59$, $a = 5$ mm, $b = 15$ mm, $t_m = 0.05$ mm, $t_d = 1.86$ mm, $d_1 = 12.52$ mm, $d_2 = 3.0$ mm, 16 metal strips). (a) 10.9 GHz. (b) 11.45 GHz. (c) 11.9 GHz.

we demonstrated the measured, calculated and target $(\sec^2)$ patterns for the cases with frequencies 10.90, 11.45, and 11.90 GHz, respectively. Although not shown here, the frequencies from 10. 9 to 11.9 GHz have the similar pattern; however, we only demonstrate several examples for the succinctness of this paper. It is apparently to see that the difference between target and measured patterns, in average, is within 1.5 dB. The maximum coverage angle of equal radiated power along a straight line is about 90 degree. Outside this range, the radiation power drastically falls off. It is noted that this antenna radiates a $\sec^2$ pattern with vertical polarization in the azimuthal direction only. It is very different with the present applications [5]–[7] having circular footprint and circular polarization.

From the radiation pattern, we may conjecture that the radiation mechanism is due to the leaky-wave phenomenon of the 1-D metal grating [8]. The wave excited by the line source is propagating along the $\pm x$ direction, and is gradually decaying during their propagation. As shown in Fig. 2, the power leaks away from the structure, becoming leaky waves with two radiation peaks in the broadside direction. However, due to the incomplete power leakage and the existence of metal side walls, the remaining power experiences multiple reflections and results in fluctuation in its radiation pattern. The curves shown in Fig. 2(a)-(c) could be used to predict the area of uniform coverage. If an imaginary plane was placed at a distance h from the antenna, the uniform coverage length along the x axis is $L_{\max} = h(cot\phi_1 + cot\phi_2)$ Where ϕ_1 and ϕ_2 are the lower and upper bounds of the azimuthal angle (in degree) satisfying the condition of uniform coverage, which could be read from Fig. 2. For example, if the distance h is 0.52 m, the maximum uniform coverage along the *x axis* will be about 1.2 m for the case shown in Fig. 2(a) with $\phi_1 = 50°$ and $\phi_2 = 130°$, respectively.

In the following example, we measured the y-direction electric-field strength on a rectangular plane in front of the antenna for the three cases with frequency 10.90, 11.45, and 11.90 GHz, respectively. The measurement setup is shown in the attached figure of Fig. 3. The distance from the antenna to the rectangular plane is 0.52 m. As shown in Fig. 3, the horizontal and vertical axes represent the position along the *x* and *y* axis, respectively. The electric-field strength is drawn in different color. From these contour maps of constant electric-field intensity, we observed that the field distribution within 6 dB variation forms a rectangular footprint for this type of shaped-beam antenna.

Fig. 4 shows the measured and calculated reflection coefficient (S_{11}) for the planar shaped-beam antenna. The impedance bandwidth $(S_{11} = -10\,\mathrm{dB})$ is around 740 MHz (from 11.26 to 12 GHz). Notably, in the theoretical formulation, we assumed that the current distribution along the excitation source is uniform. However, the nonuniform distribution of the current source may make some discrepancy between numerical and measured results.

Table I shows the radiation efficiency of this antenna operated from 11.30 to 11.80 GHz. From the table, it is obviously to see that the efficiency is gradually decreasing. We may conclude that it is mainly due to the dielectric loss coming from the dielectric slab, which is used to support the metal strips. To reduce the dielectric loss, we may employ the low-loss microwave substrate when this antenna is operated in the millimeter wave region.

In the previous examples, a planar shaped-beam antenna was fabricated, and its radiation patterns at various different operation frequencies were measured. Besides, a computer program was developed to calculate the field distribution in the structure and the far-field radiation pattern, as well. The good agreement between the measured and calculated results was obtained. Therefore, we have a good position to carry out some further numerical simulations for inspecting the parameters affecting the radiation pattern. In the following section, we not only demonstrated the calculated radiation pattern, but also numerically discussed the variation of the radiation pattern against the changes in the following parameters (sensitivity analysis), such as the metal strip width, the relative dielectric constant, thickness of the dielectric layer, number of metal strips, and the location of the excitation source. Notably, in the following examples, the radiation pattern of the planar shaped-beam antenna has been normalized to that of the line source. Moreover, since the structure is closed in the backward and sideward directions, their radiation is inconsiderably in those directions. We only demonstrated the forward radiation pattern for the following examples.

A. Effect of the Dielectric Slab Thickness on the Radiation Pattern

In Fig. 5, we changed the thickness of the dielectric substrate to see the variation on the radiation pattern. In this example, the dielectric substrate with the relative dielectric constant $\varepsilon_r = 2.59$ was used, and its thickness was varied from 0.9 to 2.9 mm. From this figure, it is apparently to see that the two radiation peaks gradually move from broadside- toward end-fire-

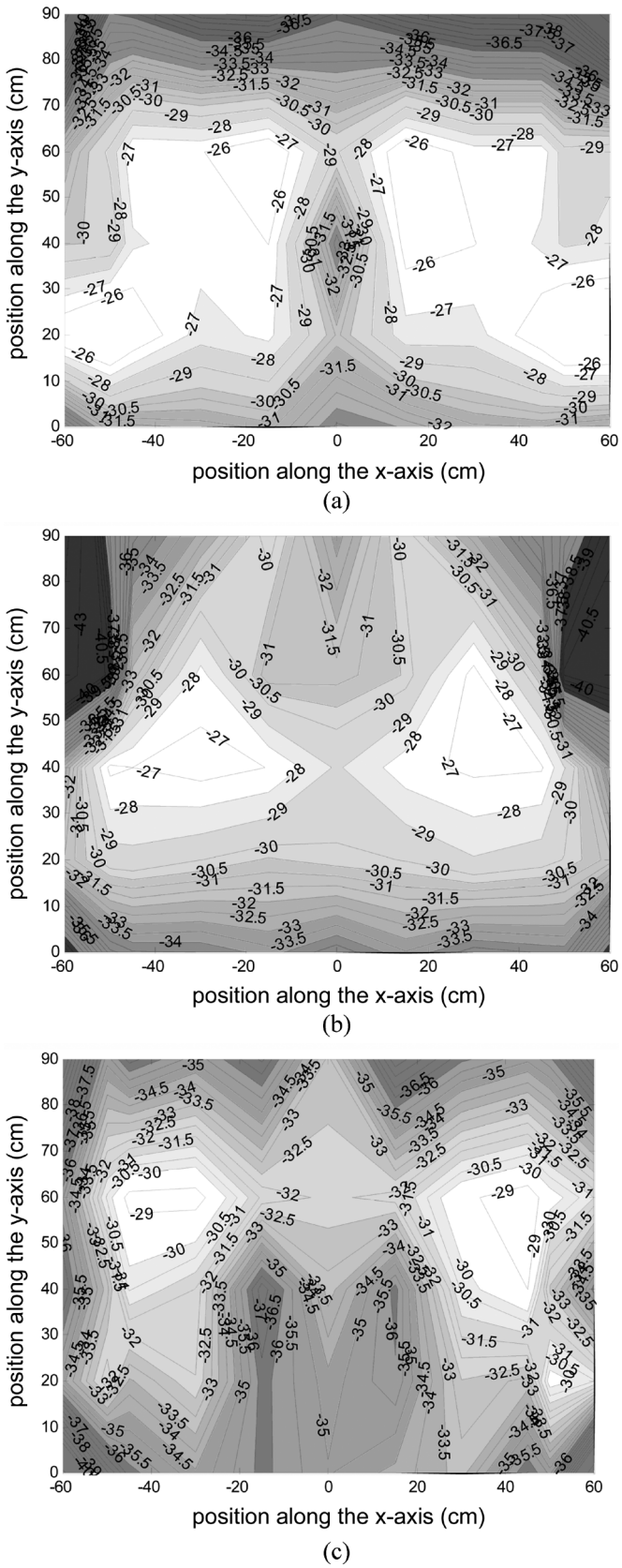

Fig. 3. Measured contour map of the y-direction electric field strength on a rectangular plane. (a) 10.90 GHz. (b) 11.45 GHz. (c) 11.90 GHz.

direction. As we have mentioned earlier, the two radiation peaks are due to the leaky wave phenomenon. The peak radiation angle

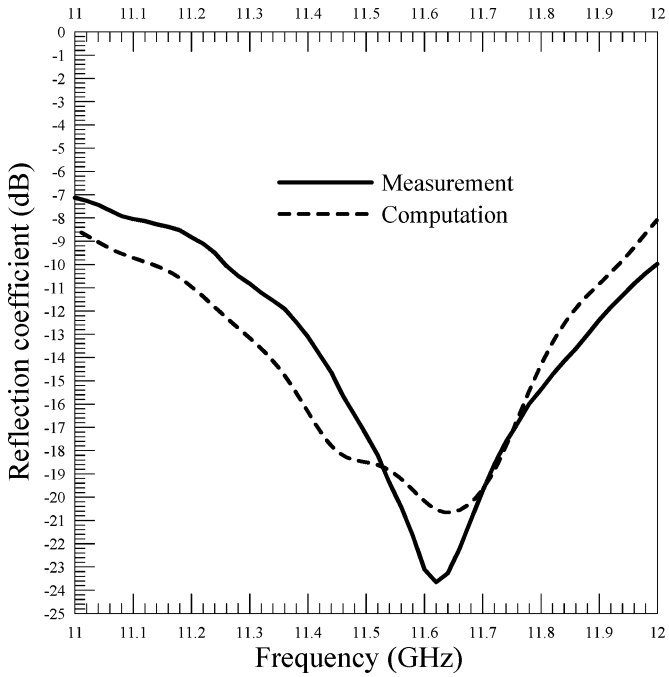

Fig. 4. Measured and calculated reflection coefficient for the shaped-beam antenna.

TABLE I
MEASURED RADIATION EFFICIENCY FOR THE SHAPED-BEAM ANTENNA

frequency (GHz)	Efficiency
11.30	75.54%
11.36	73.27%
11.42	72.58%
11.62	71.40%
11.80	70.70%

(counted from the x axis) can be roughly determined by the formula given here [8]

$$\phi = \cos^{-1}(\beta_x/k_o). \tag{14}$$

As the thickness of the dielectric layer is increasing, the average dielectric constant of the waveguide channel (the region between the metal grating and the metal plate) is increasing. Accordingly, the phase constant along the x direction is increasing, therefore, the radiation angle moves toward low-grazing angles. Moreover, as shown in this figure, the leaky-wave phenomenon gradually disappears as the dielectric layer thickness increases to 2.5 mm. We may conjecture that the thick dielectric layer causes the electromagnetic wave tend to be bound in the waveguide channel. In addition, this figure also reveals that, excluding the thick thickness cases, the shaped-beam pattern is not sensitive to the variation of dielectric thickness.

B. Effect of the Relative Dielectric Constant on the Radiation Pattern

In Fig. 6, we fixed the thickness of the dielectric layer and changed the relative dielectric constant from 1.9 to 3.3 to see the variation on the far-field pattern. Different from the previous

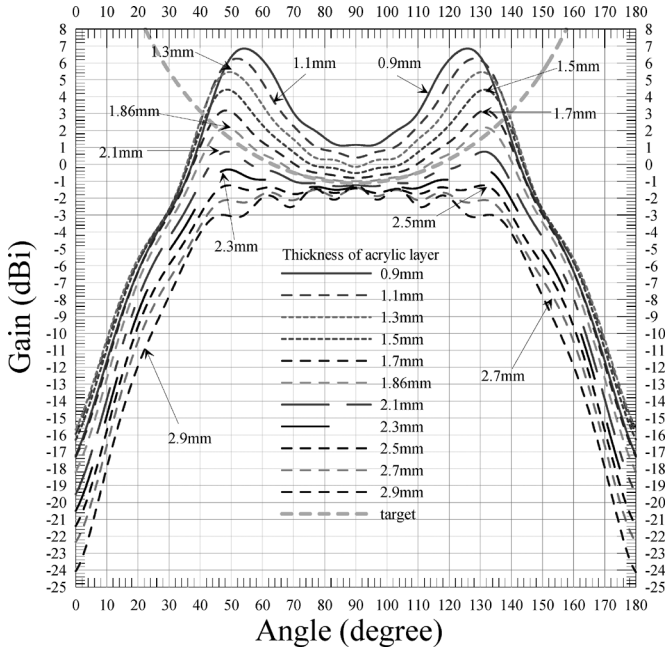

Fig. 5. Radiation pattern for different dielectric layer thicknesses at 11.43 GHz. ($\varepsilon_r = 2.59$, $a = 5$ mm, $b = 15$ mm, $t_m = 0.05$ mm, $d_1 = 12.52$ mm, $d_2 = 3.0$ mm).

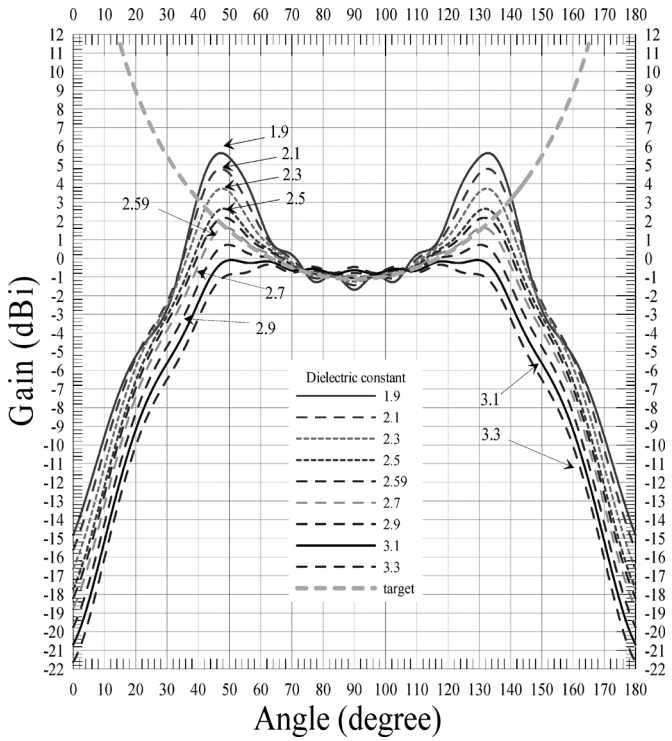

Fig. 6. Radiation pattern for different dielectric constants at 11.43 GHz. ($a = 5$ mm, $b = 15$ mm, $t_m = 0.05$ mm, $t_d = 1.86$ mm, $d_1 = 12.52$ mm, $d_2 = 3$ mm).

case, the peak radiation angles almost remain as the relative dielectric constant increases. It is instructive to know that the increase in the relative dielectric constant seems not to change the phase constant β_x. For the high relative dielectric constant cases, the waves excited by the line source may be trapped in

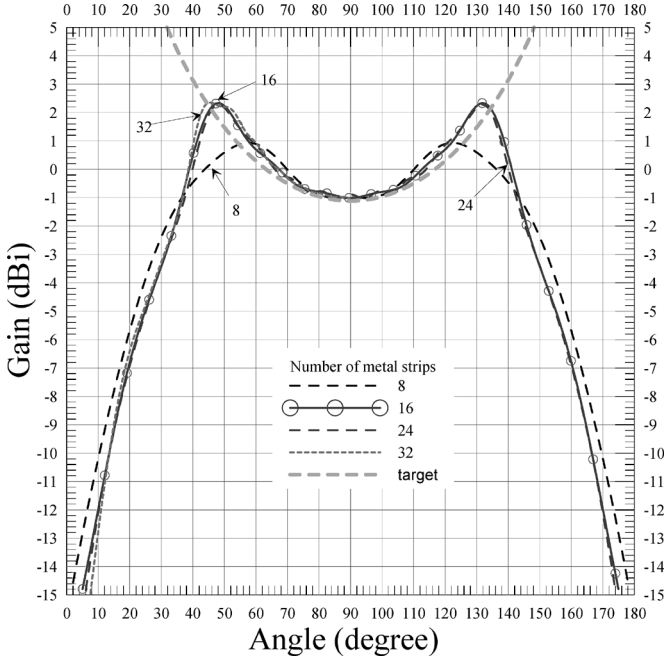

Fig. 7. Radiation pattern for different number of metal-strip array ($\varepsilon_r = 2.59$, $a = 5$ mm, $b = 15$ mm, $t_m = 0.05$ mm, $t_d = 1.86$ mm, $d_1 = 12.52$ mm, $d_2 = 3$ mm).

the waveguide channel and have a small attenuation (leaky) constant. Besides, from this figure, we observe that there are some fluctuations with the radiation pattern; particularly for the cases with relatively high dielectric constant. They are caused by the multiple reflections of the space wave, radiating directly from the line source, interacting with the dielectric layer having high dielectric constant.

C. Effect of the Number of Metal Strips on the Radiation Pattern

In this example, we change the number of metal strips to see the variation on the radiation far-field pattern. As demonstrated in Fig. 7, the radiation peak angle and strength, contributed by the leaky waves, are almost the same for the cases with 16, 24, and 32 metal strips. It is because that the phase constant along the x direction almost remains the same value as the number of periods is large enough (greater than 16 in this case).

D. Effect of the Line Source Position on the Radiation Pattern

In Fig. 8, we changed the position of the line source along the z direction to observe the variation on the far-field radiation pattern. From the previous examples, we know that the function of line source is to excite the waveguide mode propagating along the $\pm x$ direction. The propagating waveguide mode leaks its power into the surrounding medium. Since the offset of the position of line source only affect the strength of excited waveguide mode, shown in (A17), the leaky wave angles (two radiation peaks) shall be unchanged. On the other hand, the radiation intensity in the forward direction (around 90 degree) changes since it is mainly contributed by the space wave radiation directly from the line source. Thus, we may observe that the field strength is decreasing as the line source is moving toward the metal plate. It may be explained by the image theory; that is, the

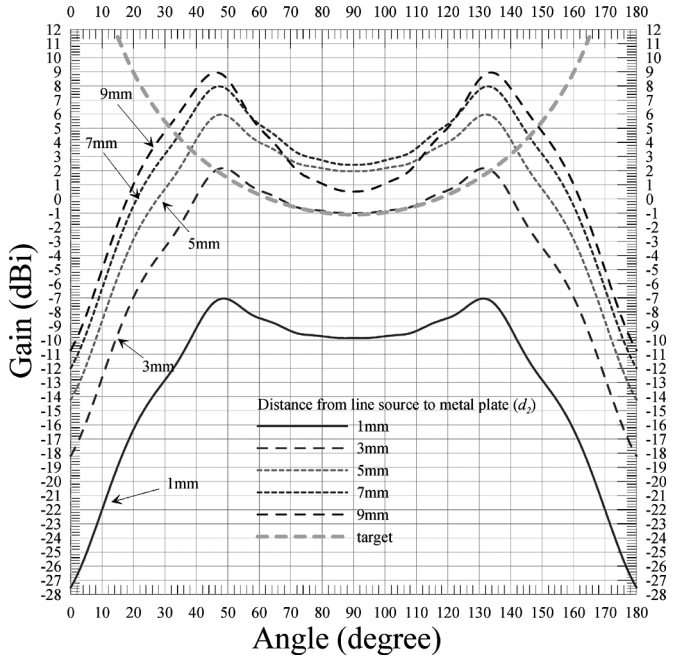

Fig. 8. Radiation pattern for different distances from the line source to meal ground plane ($\varepsilon_r = 2.59$, $a = 5$ mm, $b = 15$ mm, $t_m = 0.05$ mm, $t_d = 1.86$ mm, $d_1 = 12.52$ mm, 11.43 GHz).

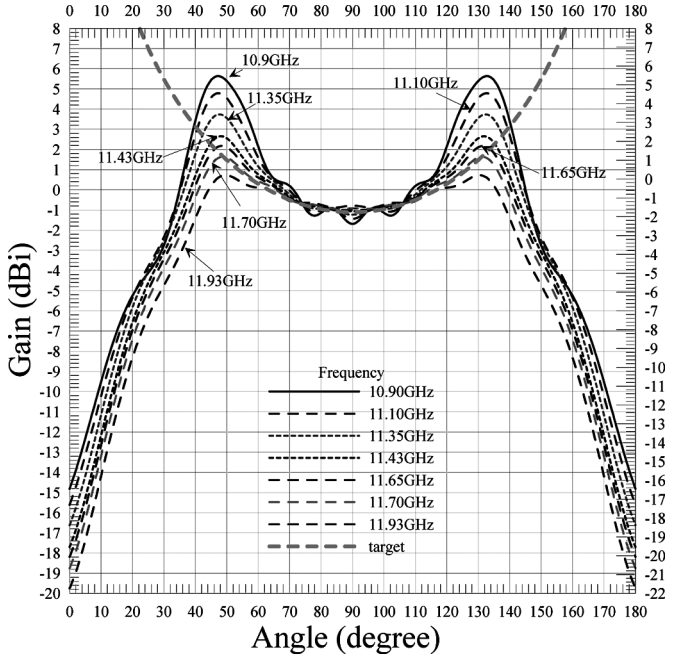

Fig. 9. Radiation pattern for various frequencies ($\varepsilon_r = 2.59$, $a = 5$ mm, $b = 15$ mm, $t_m = 0.05$ mm, $t_d = 1.86$ mm, $d_1 = 12.52$ mm, $d_2 = 3$ mm).

image line source is directed opposite to that of the line source, reducing the strength in the far field. However, according to the curves shown in this figure, the position of line source can offer us a much greater degree of flexibility in tuning the beam shape to meet the target pattern.

E. Frequency Range of Operation

In the previous examples, we have investigated some parameters affecting the radiation far-field pattern. These results reveal that this antenna has considerable tolerance in the structure parameters and dielectric constant of the dielectric slab while maintaining the desired pattern. In the following example, we scanned the operation frequency from 10.9 to 11.93 GHz to observe the variation on the radiation pattern. In doing so, the bandwidth for obtaining the desired $\sec^2$ pattern could be realized. From Fig. 9, we observed that the maximum deviation from the target pattern (angle ranges from 50° to 130°) is within 1 dB for the frequencies ranging from 11.43 to 11.93 GHz (500 MHz bandwidth). Besides, it is apparently to observe that the maximum coverage angle shrinks in the lower frequency range from 10.9 to 11.35 GHz.

V. Conclusion

In this paper, the prototype of a linear-polarized planar antenna radiating a rectangular footprint of uniform electric-field strength was presented. Combining the forward-, backward-, leaky-wave and space wave radiation characteristics, the highly shaped-beam $(\sec^2)$ pattern in the azimuthal plane was achieved. We have fabricated the antenna and measured its radiation characteristics. The bandwidth for maintaining a $\sec^2$ pattern (covering 80 degree) in the azimuthal plane is around 500 MHz. The rigorous mode-matching method incorporating the equivalent principle was employed to compute the far-field radiation pattern. The good agreement between the numerical and measured results was obtained. Furthermore, we have carried out the sensitivity analyses for the radiation pattern with respect to the changing in structure parameters and permittivity of the dielectric slab. Although the present antenna cannot have the radiation characteristics of circular footprint coverage and circular polarization, it provides an alternative idea in synthesizing the highly shaped-beam pattern using leaky-wave characteristics of a periodic structure. The further work is to generate leaky waves along each radius direction on a circular aperture to produce circular footprint coverage.

Appendix

After collecting the modal- voltage and current in respective PPWGs, we could rewrite the (8)–(10) in terms of matrix-vector form given here

$$\underline{V}\left(t_m^+\right) = \sum_{i=1}^{N} \mathbf{R}^{(i)} \overline{\underline{V}}^{(i)}\left(t_m^-\right) \tag{A1}$$

$$\overline{\underline{V}}^{(i)}\left(t_m^-\right) = \overline{\mathbf{R}}^{(i)} \underline{V}\left(t_m^+\right) \tag{A2}$$

$$\overline{\underline{I}}^{(i)}\left(t_m^-\right) = \overline{\mathbf{R}}^{(i)} \underline{I}\left(t_m^+\right) \tag{A3}$$

where the parameter i denotes the index number of the ith aperture in the metal grating and the parameter N is the number of apertures. Parameter $\mathbf{R}^{(i)}$ is a coupling matrix, representing the electromagnetic field coupling between the oversized parallel-plate waveguide and the ith subparallel-plate waveguide, with its mn^{th} element given by

$$r_{mn}^{(i)} = \left\langle \phi_m(x) \middle| \overline{\phi}_n^{(i)}(x) \right\rangle. \tag{A4}$$

In addition, $\overline{\mathbf{R}}^{(i)}$ represents the transpose of matrix $\mathbf{R}^{(i)}$.

Having the relationship between the voltage and current waves in uniform dielectric layer and metal grating at the junction discontinuities, we could then develop the input-output relation of a metal grating layer, including the input impedance matrix and the voltage transfer matrix. First, if the output admittance matrix of the metal grating layer is given by

$$\underline{I}\left(t_m^+\right) = \mathbf{Y}_l \underline{V}\left(t_m^+\right) \tag{A5}$$

where t_m^+ represents the output surface position of the metal grating, in the oversized waveguide region. Substituting (A5) into (A1), (A2), and (A3), we could obtain the output admittance matrix at $z = t_m^-$, which is given

$$\overline{I}\left(t_m^-\right) = \overline{\mathbf{Y}}_l \overline{V}\left(t_m^-\right) \tag{A6}$$

$$\text{with} \quad \overline{\mathbf{Y}}_l = \overline{\mathbf{R}} \mathbf{Y}_l \mathbf{R}. \tag{A7}$$

$$\text{with} \quad \mathbf{R} = (\mathbf{R_1}\ \mathbf{R_2}\ \ldots\ \mathbf{R_{N-1}}\ \mathbf{R_N}) \tag{A8}$$

where the super-matrix $\mathbf{R}$ contains each of the partition matrix $\mathbf{R}^{(i)}$. The super-vectors $\underline{V}$ and $\underline{I}$ were obtained by collecting each $\underline{V}^{(i)}$ and $\underline{I}^{(i)}$, respectively.

It can be shown, through a rather lengthy and involved derivation, we could obtain the input impedance matrix at $z = 0^+$, which is defined in the metal grating layer, given as

$$\overline{\mathbf{Z}}_{in}(0^+) = (\mathbf{I} + \overline{\mathbf{\Gamma}})(\mathbf{I} - \overline{\mathbf{\Gamma}})^{-1} \overline{\mathbf{Z}}_o \tag{A9}$$

$$\overline{\mathbf{\Gamma}} = \exp(-j\overline{\mathbf{k}}_z t_m) \overline{\mathbf{\Gamma}}_l \exp(-j\overline{\mathbf{k}}_z t_m) \tag{A10}$$

$$\overline{\mathbf{\Gamma}}_l = (\overline{\mathbf{Y}}_l + \overline{\mathbf{Y}}_o)(\overline{\mathbf{Y}}_o - \overline{\mathbf{Y}}_l)^{-1} \tag{A11}$$

$$\overline{\mathbf{T}}\left(t_m^+ \to 0^+\right) = (\mathbf{I} + \overline{\mathbf{\Gamma}}_l) \exp(-j\overline{\mathbf{k}}_z t_m)(\mathbf{I} - \overline{\mathbf{\Gamma}})^{-1} \tag{A12}$$

where $\overline{\mathbf{Z}}_o$ is a super-matrix containing each partition matrix $\overline{\mathbf{Z}}_o^{(i)}$ in each sub parallel-plate waveguide. The parameter $\overline{\mathbf{k}}_z$ is also a super diagonal matrix with each element representing the z-direction propagation constant of each mode in each sub parallel-plate waveguide. The matrix $\overline{\mathbf{T}}$ defines the relationship for the voltage waves at the input and output interfaces of the metal grating layer, which is given

$$\overline{V}\left(t_m^+\right) = \overline{\mathbf{T}}\left(t_m^+ \to 0^+\right) \overline{V}(0^+). \tag{A13}$$

Moreover, the input impedance, defined at the input interface in the oversized waveguide region, and the transfer matrix, defining the relationship between the output and input voltage waves through the metal grating layer, are given as follows:

$$\mathbf{Z}_{in}(0^-) = \mathbf{R} \mathbf{Z}_{in}(0^-) \overline{\mathbf{R}} \tag{A14}$$

$$\mathbf{T}\left(t_m^+ \to 0^-\right) = \mathbf{R} \overline{\mathbf{T}}\left(t_m^+ \to 0^+\right) \overline{\mathbf{R}} \tag{A15}$$

where the matrix $\mathbf{T}$ satisfy

$$\underline{V}\left(t_m^+\right) = \mathbf{T}\left(t_m^+ \to 0^-\right) \underline{V}(0^-). \tag{A16}$$

A. Radiation Far-Field Calculation Using Equivalent Principle

In addition to the input-output relationship of a metal-strip array layer, the input-output relation of a uniform dielectric layer filled in a parallel-plate waveguide could be obtained and be expressed in a similar form as shown in (A9). Since it is well known and could be found in the literature, we neglect it in this section.

As aforementioned, this antenna is excited by a current source. The line source embedded in the air separating layer could be expressed in terms of the superposition of parallel-plate waveguide modes, each of which is viewed as the incident mode for the scattering analysis. The modal voltage waves at the position of line source could be written as

$$\underline{V}(z = -t_d - d_1 + d_2) = (\mathbf{Y}_{up} + \mathbf{Y}_{dn})^{-1} I_o \underline{\phi}(x') \tag{A17}$$

where $\mathbf{Y}_{\rm up}$ and $\mathbf{Y}_{\rm dn}$ are the input admittance matrices looking upward and downward from the position of line source, respectively. The parameter I_o is the amplitude of current source. The vector $\underline{\phi}$ is the vector containing each of the mode function evaluated at $x = x'$, $\{\phi_n(x')\}$.

REFERENCES

[1] A. A. Kishk, "Simple primary focus feeds for deep reflector," *Proc. Inst. Elect. Eng.*, vol. 136, pp. 169–171, Apr. 1989.

[2] S. G. Hay, D. G. Bateman, T. S. Bird, and F. R. Cooray, "Simple Ka-band Earth coverage antennas for LEO satellites," in *IEEE Antennas Propag. Soc. Int. Symp.*, Jul. 1999, vol. 1, pp. 11–16.

[3] A. D. Olver, P. J. B. Clarricoats, A. A. Kishk, and L. Shafai, *Microwave Horns and Feeds*. New York: IEEE, 1994.

[4] T. S. Bird, J. S. Kot, N. Nikolic, G. L. James, and S. J. Barker, "Millimeter-wave antenna and propagation studies for indoor wireless LANs," in *Antennas Propag. Soc. Int. Symp.*, Jun. 1994, vol. 1, pp. 336–339.

[5] P. F. M. Smulders, S. Khusial, and M. H. A. J. Herben, "A shaped reflector antenna for 60-GHz indoor wireless LAN access points," *IEEE Trans. Veh. Technol.*, vol. 50, pp. 584–591, Mar. 2001.

[6] P. F. M. Smulders and M. H. A. J. Herben, "A shaped reflector antenna for 60-GHz radio access points," *IEEE Trans. Antennas Propag.*, vol. 49, pp. 1013–1015, Jul. 2001.

[7] A. Kumar, "Antennas for wireless indoor millimeter-waves applications," in *Proc. IEEE CCECE*, May 2003, vol. 3, pp. 1877–1880.

[8] C. A. Balanis, *Antenna Theory: Analysis and Design*. New York: Wiley, 1997.

[9] H.-Y. D. Yang and D. R. Jackson, "Theory of line-source radiation from a metal-strip grating dielectric-slab structure," *IEEE Trans. Antennas Propag.*, vol. 48, no. 4, pp. 556–564, Apr. 2000.

[10] F. Capolino, D. R. Jackson, and D. R. Wilton, "Fundamental properties of the field at the interface between air and a periodic artificial material excited by a line source," *IEEE Trans. Antennas Propag.*, vol. 53, pp. 91–99, Jan. 2005.

[11] F. Capolino, D. R. Jackson, and D. R. Wilton, "Mode excitation from sources in two-dimensional EBG waveguides using the array scanning method," *IEEE Microw. Wireless Compon. Lett.*, vol. 15, pp. 49–51, Feb. 2005.

[12] G. Lovat, P. Burghignoli, F. Capolino, D. R. Jackson, and D. R. Wilton, "Analysis of directive radiation from a line source in a metamaterial slab with low permittivity," *IEEE Trans. Antennas Propag.*, vol. 54, pp. 1017–1030, May 2006.
[13] T. Zhao, D. R. Jackson, J.T. Williams, H.-Y. D. Yang, and A. A. Oliner, "2-D periodic leaky-wave antennas- part I: Metal patch design," *IEEE Trans. Antennas Propag.*, vol. 53, pp. 3505–3514, Nov. 2005.
[14] G. Lovat, P. Burghignoli, and D. R. Jackson, "Fundamental properties and optimization of broadside radiation from uniform leaky-wave antennas," *IEEE Trans. Antennas Propag.*, vol. 54, pp. 1442–1452, May 2006.
[15] J. Vazquaz, M. Shelley, and P. De Maagt, "Parallel plate photonic bandgap and periodic medium waveguides," in *Inst. Elect. Eng. 11th Int. Conf. Antennas Propag. ICAP2001*, Manchester, U.K., Apr. 17–20, 2001, pp. 315–318.
[16] D. R. Jackson, A. A. Oliner, and A. Ip, "Leaky-wave propagation and radiation for a narrow-beam multiple-layer dielectric structure," *IEEE Trans. Antennas Propag.*, vol. 41, pp. 344–348, Mar. 1993.
[17] L. Leger, T. Monediere, and B. Jecko, "Enhancement of gain and radiation bandwidth for a planar 1-D EBG antenna," *IEEE Microw. Wireless Compon. Lett.*, vol. 15, no. 9, pp. 573–575, Sep. 2005.
[18] A.R. Weily, L. Horvath, K.P. Esselle, B.C. Sanders, and T.S. Bird, "A planar resonator antenna based on a woodpile EBG material," *IEEE Trans. Antennas Propag.*, vol. 53, pp. 216–223, Jan. 2005.

Ruey Bing Hwang (M'96–SM'06) was born in Nantou, Taiwan, R.O.C., on January 20, 1967. He received the B.S. degree in communication engineering and the Ph.D. degree in electronics from National Chiao-Tung University, Hsinchu, Taiwan, R.O.C., in 1990 and 1996, respectively, and the Master's degree in electrical engineering from National Taiwan University, Taipei, in 1992.

In 1996, he joined the National Center of High Performance Computing, Hsinchu, as an Associate Research Scientist. From 1999 to 2000, he was a Postdoctoral Research Fellow with the National Chiao-Tung University, where, from fall 2000 to spring 2002, he was a Research Associate Professor with the Microelectronics and Information Systems Research Center. From spring 2002 to summer 2004, he was an Associate Professor with the Graduate Institute of Communication Engineering, National Chi Nan University, Nantou, Puli, Taiwan, R.O.C. In August 2004, he joined the faculty of the Department of Communication Engineering, National Chiao Tung University. His research interests include the guiding and scattering characteristics of periodic structures (or photonic crystals), meta-materials, waveguide antennas, array antennas design, and electromagnetic compatibility.

Dr. Hwang is a Member of Phi Tau Phi.

Ta Chun Pu was born in Taiwan, R.O.C., on March 8, 1978. He received the B.S.E.E. and M.S.E.E. degrees from National Sun Yat-Sen University, Kaohsiung, Taiwan, R.O.C., in 2000 and 2002, respectively.

He is currently working toward the Ph.D. degree at National Chiao Tung University, Hsinchu, Taiwan, R.O.C. His research interests include the guiding and scattering characteristics of periodic structures and shaped-beam antenna design.